An In Situ Hyaluronic Acid-Fibrin Hydrogel Containing Drug-Loaded Nanocapsules for Intra-Articular Treatment of Inflammatory Joint Diseases

Nataliya Storozhylova, José Crecente-Campo, David Cabaleiro, Luis Lugo, Christophe Dussouy, Sandra Simões, Madalena Monteiro, Cyrille Grandjean, María J Alonso

Regenerative Engineering and Translational Medicine
DOI: 10.1007/
Article type: Original Research

An *in situ* hyaluronic acid-fibrin hydrogel containing drug-loaded nanocapsules for intra-articular treatment of inflammatory joint diseases

Nataliya Storozhylova[1,3], José Crecente-Campo[1], David Cabaleiro[2], Luis Lugo[2], Christophe Dussouy[3], Sandra Simões[4], Madalena Monteiro[5], Cyrille Grandjean[3], María J. Alonso[1*]*

[1]Dr. Nataliya Storozhylova, Dr. José Crecente-Campo, Prof. María J. Alonso
Center for Research in Molecular Medicine and Chronic Diseases (CIMUS), Department of Pharmacology, Pharmacy and Pharmaceutical Technology, Universidade de Santiago de Compostela, Campus Vida, Santiago de Compostela, 15782, Spain

[2]Dr. David Cabaleiro, Dr. Luis Lugo
Department of Applied Physics, Faculty of Science, University of Vigo, Vigo, 36310, Spain

[3]Dr. Nataliya Storozhylova, Dr. Christophe Dussouy, Dr. Cyrille Grandjean
Université de Nantes, CNRS, UFIP, UMR 6286, F-40000 Nantes, France

[4]Dr. Sandra Simões
Research Institute for Medicines, Faculty of Pharmacy, Universidade de Lisboa, Lisboa, 1649-003, Portugal

[5]Dr. Madalena Monteiro
Laboratório de Patologia, Instituto Nacional de Investigação Agrária e Veterinária, Oeiras, 2780-157, Portugal

* Corresponding authors: María J. Alonso (mariaj.alonso@usc.es) and José Crecente-Campo (jose.crecente@usc.es)

Abstract

Intra-articular (IA) administration of drugs is an appealing route for the effective treatment of large joint diseases. However, a key limitation of this route is the premature elimination of the injected drugs from the synovial cavity. The objective of this work was to develop an easily injectable controlled release system intended to prolong the activity of anti-inflammatory drugs in the articular cavity. The system was an *in situ* forming hydrogel, made of fibrin and hyaluronic acid (HA), loaded with nanocapsules (NCs). The NCs, consisting of an olive oil core surrounded by a HA shell, were loaded with two different drugs, dexamethasone (DMX) and a galectin-3 inhibitor. They presented a particle size in the range of 122-135 nm and a surface charge of −29/−31 mV. The gelation time, rheological properties and porosity of the system could be adjusted by different parameters, such as addition of fibrin crosslinkers factor XIII and α2-antiplasmin. The non-crosslinked HA-fibrin hydrogels containing 30% (v/v) NCs showed the capacity to control the release of the encapsulated drug, DMX, for 72 h in simulated synovial fluid. The preliminary *in vivo* evaluation of the system containing a galectin-3 inhibitor in an acute synovitis rat model, showed a suppression of inflammation after IA administration compared with the non-treated control. In brief, this work shows the possibility to combine an

in situ forming hydrogel and NCs as a drug delivery strategy for IA administration and suggests its potential for the treatment of arthropathies.

Graphical Abstract

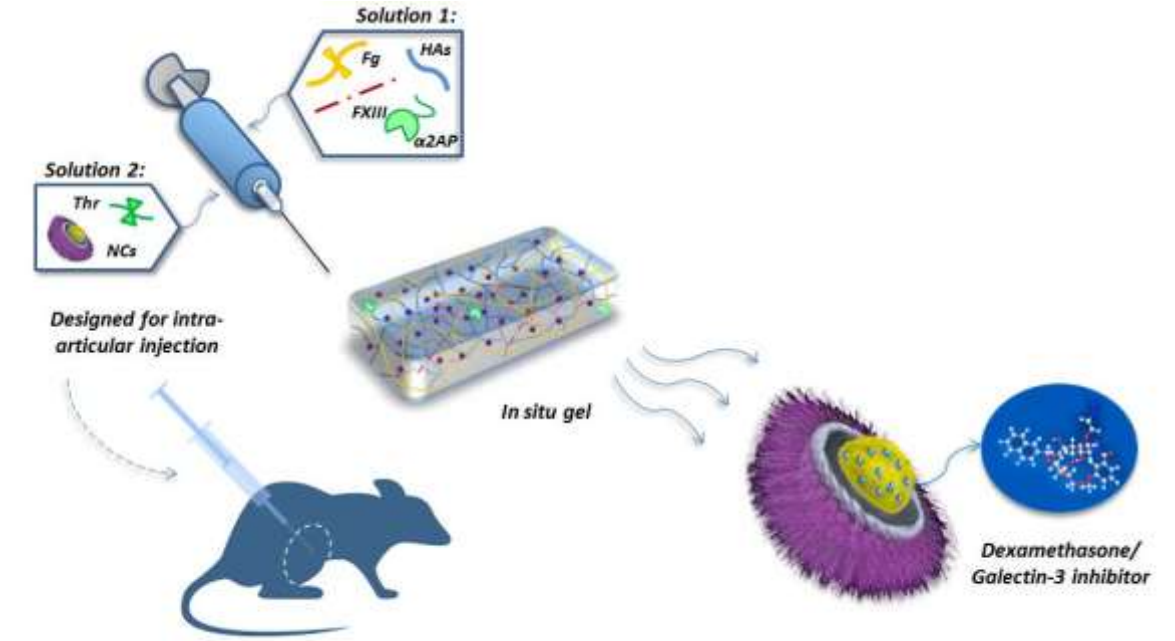

α2-AP - α2-antiplasmin, Fg- Fibrinogen, FXIII -Factor XIII, HAs - Hyaluronic acids, NCs – Nanocapsules, Thr – Thrombin.

Lay Summary

This work describes the development and characterization of a new *in situ* forming hydrogel adapted for intra-articular administration of anti-inflammatory drugs. The prolonged local delivery of these drugs is expected to improve the treatment of large joints arthropathies. To achieve this objective the hydrogel, made of biodegradable materials, was loaded with nanodeposits of drugs, named nanocapsules. The efficacy of the system, containing a new galectin-3 inhibitor as a drug candidate, was tested in a rat model of acute synovial inflammation. These results represent the first insights on the *in vivo* activity of a new galectin-3 inhibitor on a potential galectin-3 immunotherapeutic target for inflammatory joints diseases.

Keywords: intra-articular drug delivery, *in situ* hydrogel, nanocapsules, arthropathies, galectin-3 inhibitor.

1. Introduction

The intra-articular (IA) modality of administration is particularly attractive for the treatment of joint diseases, however, it remains challenging due to the rapid efflux of injected drugs from the articular cavity through the synovial capillaries and/or the lymphatic vessels [1,2]. IA drug delivery systems, including micro-/nanoparticles and hydrogels, and a combination of them, have been developed to prolong the drugs residence time in the joint cavity, reducing systemic exposure and, hence, off-target effects [3–5].

With regard to the use of micro- and nanotechnologies for IA drug delivery, liposomes [6,7] metallic [8] and polymeric micro-/nanoparticles [9,10] containing anti-inflammatory [11,12] or disease-modifying anti-rheumatic drugs [13,14] have overall resulted in improved PK/PD and efficacy/toxicity profiles, as compared to the free drugs [1,10,15]. From the translational perspective, the result has led to the marketing of two formulations for the treatment of inflammatory osteoarthritis (OA), namely Lipotalon® (a liposomal dexamethasone 21-palmitate) [16] and Zilretta® (PLGA microspheres, containing triamcinolone acetonide), the last one providing a therapeutic effect, maintained for up to 24 weeks [17].

On the other hand, hydrogels, marketed as viscosupplements for OA and rheumatoid arthritis (RA) treatment [18,19], have also been explored for the controlled delivery of drugs. For example, a crosslinked hyaluronic acid (HA) gel containing dexamethasone (DXM) showed an anti-inflammatory and chondroprotective effect for 8 weeks after the injection in an OA rat model [20]. However, a limitation of these hydrogels is related to their high viscosity, which often leads to an increase in IA pressure and pain in the knee joint [21]. This limitation has opened the door to the development of easily injectable *in situ* forming hydrogels. As an example, a thermosensitive triblock poly(ε-caprolactone-co-lactide)-*b*-poly(ethylene glycol)-*b*-poly(ε-caprolactone-co-lactide) copolymer hydrogel, loaded with celecoxib, showed sustained local release for 4 weeks in healthy horses [22].

Recent attention has been paid to more advanced formulations, which consist of combinations of drug loaded micro-/nanocarriers with hydrogels [23–25]. For example, the thermo-responsive Pluronic® F127 loaded with chitosan nanoparticles, used for the IA co-delivery of kartogenin and diclofenac, showed a 2-week retention time of the drugs in the joints [13]. Nevertheless, the work of *in situ* forming hydrogels containing drug-loaded micro-/nanocarriers is at a very early stage, with only a few candidates being tested *in vivo* [4,22] most of them in healthy animals, thus, their residence time and prolonged release at inflamed joints remains unknown.

In this study, we report the development of an *in situ* forming hydrogel containing drug loaded NCs, intended for the treatment of joint inflammation. In order to modulate the rheological properties of the hydrogel made of HA and fibrin, fortifying agents, namely factor XIII (FXIII) and α2-antiplasmin (α2AP), were added to the gel. NCs were designed to serve as reservoirs for lipophilic drugs, i.e. DXM (used in this study as a model anti-inflammatory corticosteroid drug) and a novel galectin-3 inhibitor (Gal-3i) [26,27]. This drug candidate loaded into the drug delivery system was developed to target the extracellular protein galectin-3 (Gal-3), identified recently as a primer trigger of the pro-inflammatory cascade in arthritis [28,29]. The resulting system was evaluated *in vitro* and also *in vivo* for its efficacy in an acute synovitis rat model.

2. Materials and Methods

Fibrinogen and thrombin from human blood plasma were purchased from Sigma-Aldrich (St. Louis, MO). Sodium hyaluronate (HA) of different average MW 40 kDa, 700 kDa, 1.5 MDa were acquired from Lifecore Biomedical (Chaska, MN). FXIII and α2AP from human blood plasma were obtained from Haematologic Technologies, Inc. (Essex Junction, VT) and Lee Biosolutions, Inc. (Maryland Heights, MO), correspondingly. Dexamethasone (DXM) was purchased from Acofarma (Terrassa, Spain). The phosphatidylcholine enriched soy lecithin (EPIKURON® 145 V) was a kind gift from Cargill (Hamburg, Germany). Virgin olive oil was purchased from Acros Organics (Geel, Belgium). Oleylamine, Nile red, HEPES, BSA, sodium chloride, calcium chloride dihydrate, potassium chloride, sodium phosphate dibasic and potassium phosphate monobasic were acquired from Sigma-Aldrich (St. Louis, MO). All the testing materials were obtained in sterile conditions using of endotoxin-free water and all other ingredients and organic solvents were of analytical grade. The laboratory glassware used for *in vivo* formulations preparation was previously sterilized by autoclave (Systec, Wettenberg, Germany).

Animals

Sprague-Dawley rats (200/225 g) were acquired from Charles River, Germany. They were used after 1-week acclimatization to the laboratory environment and housed in polypropylene cages (5 per cage) under standard controlled conditions (20-24 °C, 55 ± 5% relative humidity, 12 h light/dark cycle), were fed and had access to water *ad libitum*. All animal studies were carried out according to the animal welfare organ of the Faculty of Pharmacy, University Lisbon, approved by the competent national authority Direção-Geral de Alimentação e Veterinaria (DGAV) and in accordance with the EU Directive (2010/63/EU), the Portuguese laws (DL 113/2013, 2880/2015, 260/2016 and 1/2019) and all relevant legislation.

Preparation of HA NCs

HA NCs were prepared by the solvent displacement technique [30]. Briefly, soy lecithin (5.625 mg), oleylamine (1.125 mg) and olive oil (30 mg) were dissolved in 5 mL of ethanol. For labelled NCs, Nile Red (0.125 mg) was also included to this phase. In the case of drug loaded NCs, DXM (2.5-8.1 mg) or Gal-3i (2.5-5 mg) were incorporated to the ethanol. Then, the organic phase was injected under pressure through a needle (23G) to 10 mL of aqueous phase containing 2.5 mg of HA 700 kDa, and kept under magnetic stirring at 900 rpm during 10 minutes at room temperature. The elimination of organic solvent was performed by evaporation under vacuum (Rotavapor Heidolph, Germany) and the final volume was adjusted to 5 mL with ultrapure water. Thereafter, the NCs were isolated by ultracentrifugation (Avanti® J-E, Ultracentrifuge, Beckman Coulter, Inc., CA) at 30,000×*g* for 1 h at 15 °C.

Physicochemical and morphological properties of HA NCs

The mean size and polydispersity index (PDI) of the HA NCs were measured after dilution (100×) with ultrapure water by dynamic light scattering (DLS) at 25 °C with an angle detection of 173°. The zeta potential (ζ) was measured by laser Doppler anemometry (LDA) after diluting the samples (1:100) with ultrapure water. Both DLS and LDA analysis were performed in a Zetasizer®, NanoZS, Malvern Instruments, Malvern, UK. Particle size distribution and morphology were evaluated by transmission electron microscopy (TEM) using a JEOL JEM-2010 microscope, 200 kV, resolution: 0.23 nm (Tokyo, Japan). Samples for TEM analysis were diluted (1:20), deposited on a copper grid, stained with a phosphotungstic acid solution

(2% w/v) and allowed to dry overnight prior to analysis. The pH of the formulations was measured at Sartorius Basic Meter PB-11, Sartorius AG, Germany.

Determination of a drug concentration in the formulation

The DXM or Gal-3i concentration was determined after the isolation of the NCs by ultracentrifugation at 30,000×*g* for 1 h at 15 °C (Avanti® J-E, Ultracentrifuge, Beckman Coulter, Inc., CA). The amount of the free drug in the undernatant was quantified by high-performance liquid chromatography (HPLC), described below. For the extraction of the drug 0.1 mL of sample were mixed with 0.9 mL ethanol/acetonitrile (ACN) and kept under magnetic stirring overnight to obtain a clear solution. The samples were analyzed by HPLC, using methods adapted from the literature [31,32]. The HPLC system consisted of a VWR-Hitachi LaChrom Elite® system equipped with a UV detector L-2400 set at 239 nm (for DXM) or 254 nm (for Gal-3i) and a reverse phase SunFire column 186002560, 100Å, C18 (4.6 ID × 250 mm, pore size 5 μm), Waters, USA. For DXM quantification the mobile phase was a mixture of methanol and ultrapure water (65:35, v/v) and for Gal-3i quantification, the mobile phase was a mixture of ACN and ultrapure water (60:40, v/v), both isocratic, and the flow rate was 1 mL/min. The column was set at 30 °C and the injection volume was 20 μL. The standard calibration curves of DXM/Gal-3i were linear in the range of 1-1000 μg/mL (r^2 = 0.999). The concentration of DXM or Gal-3i in the aliquots was used to calculate the free amount of drugs and the concentration in the final system.

Preparation of HA-fibrin *in situ* forming hydrogels

The HA-fibrin *in situ* hydrogels matrixes were obtained by thrombin-activated enzymatic polymerization. Lyophilized powder of fibrinogen from human plasma was dissolved in 0.15 M solution of NaCl at 37 °C to a final concentration of 25 mg/mL, aliquoted and stored at -20 °C. Before each experiment, an aliquot was thawed at 37 °C for 30 min and was maintained at 37 °C no more than 2 hours. Further, lyophilized powder of thrombin from human plasma was dissolved in cooled to 4 °C PBS buffer (0.01 M Na_2HPO_4, 0.0018 M KH_2PO_4, 0.137 M NaCl, and 0.0027 M KCl, pH 7.2) to a final concentration of 100 NIH-U/mL. According to the National Institute of Health standard for the calibration of commercial thrombin reagents, 1 NIH-U = 0.324 ± 0.073 μg (9.0 nM). Additionally, 1% (w/v) solution of BSA was added as stabilizing agent. This thrombin solution was aliquoted and stored at -20 °C. Before each experiment the aliquot was thawed on an ice plate. HA of different MW 40 kDa, 700 kDa and 1.5 MDa was dissolved at 37 °C in a polymerization buffer (0.02 M HEPES, 0.1 M NaCl, pH 7.4) containing different amounts of Ca^{2+} (10^{-3} M and 10^{-4} M), reaching concentrations of 0.1%, 0.25%, 0.5% and 0.65% (w/v). Additionally, HA mixed solutions 0.5% and 0.65% (w/v) made from HA 700 kDa:HA 1.5 MDa = 1:1 were prepared. FXIII from human blood plasma was aliquoted and kept in 50% glycerol, 0.5 mM EDTA at concentration 5.1 mg/mL at -80 °C. Lyophilized powder of α2AP from human blood plasma was dissolved in PBS buffer + 1% (w/v) BSA as carrier and stored at concentration 0.1 mg/mL at -20 °C.

The hydrogel preparation started by testing the gelation time of fibrinogen by the action of thrombin. For that purpose, a stock solution of fibrinogen was added to the "polymerization buffer 10^{-4} M Ca^{2+}" to final concentration 1 mg/mL and by the action of thrombin in the range of concentrations 0.1-2 NIH-U/mL was converted to the gel. Later, we tested the influence of HA on fibrin gelation. Fibrinogen at a fixed concentration of 1 mg/mL was mixed with HA solutions of 40 kDa, 700 kDa and 1.5 MDa and their mixtures at concentrations of 0.1%, 0.25%, 0.5% (w/v) in "polymerization buffer 10^{-4} M Ca^{2+}" gelated upon addition of thrombin in the range of concentrations 0.1-1 NIH-U/mL. Finally, 0.5% (w/v) mixture of HA 700 kDa:HA 1.5

MDa = 1:1 was selected to enable syringeability due to moderate viscosity and postponed gelation time.

To formulate fortified HA-fibrin hydrogel FXIII at final concentration 10 µg/mL and α2AP at final concentration 0.14 µg/mL were added to the fibrinogen (1 mg/mL) and HAs 0.5% (w/v) mixture 700 kDa:1.5 MDa = 1:1 in "polymerization buffer 10^{-4} M Ca^{2+}". Thrombin was added as the last component at 0.75-1 NIH-U/mL to initiate the polymerization.

Loading of HA NCs into the hydrogel

The maximum loading of isolated HA NCs to *in situ* hydrogels was obtained for non-fortified and fortified HA-fibrin hydrogels. Prior the experiments aliquots of fibrinogen, HAs Mix 1:1 = 700 kDa:1.5 MDa solutions in polymerization buffer containing different amounts of Ca^{2+} (10^{-3} M and 10^{-4} M) and blank or drug loaded HA NCs were warmed up at 37 °C for 30 min. This formulation was named a non-fortified HA-fibrin hydrogel. **Table 1** (entries 1-4) indicates the final concentration of each ingredient of a non-fortified hydrogel. FXIII 10 µg/mL and α2AP 0.14 µg/mL were only used in case of fortified HA-fibrin hydrogels (**Table 1**, entries 1-6). The polymerization reaction was initiated by thrombin (1-2 NIH-U/mL). The hydrogel capacity to accommodate NCs was tested in the range of 10-50%.

Table 1. Composition of HA-fibrin hydrogel with NCs.

N	Composition	Final concentration
1	Fibrinogen	1.5 mg/mL
2	Thrombin *(added as a last component)*	2 NIH-U/mL
3	HAs mix 1:1 (1.5 MDa:700 kDa) in HEPES buffer, 10^{-3} M Ca^{2+}, pH 7.4	0.5%
4	NCs	30%
5	FXIII	10 µg/mL
6	α2AP	14 µg/mL

Determination of the hydrogel gelation time

The lag-time and the gelation point were performed by turbidity analysis using UV-Vis scanning spectrophotometry (Manual Beckman-Coulter DU®730 spectrophotometer, Brea, CA). The device was set up at the mode, allowing the measurement of the absorbance at 350 nm each 10 s within 20 min, recording the kinetics of the polymerization.

The gelation point of blank and NCs-loaded hydrogels was additionally measured in rheology studies, described further.

Syringeability studies

For this analysis, compositions of non-fortified and fortified HA-fibrin hydrogels containing HA NCs were transferred to the syringe Terumo Myjector U-100 Insulin with 29G needle; thrombin was added as the last component and mixed again before injection to the vial filled with PBS buffer (1:1) at 37 °C.

Porosity and surface morphology

The samples for SEM were prepared by the injection of blank and 30% NCs-loaded non-fortified and fortified HA-fibrin hydrogels to PBS buffer 1:1 and 1:1.73 (v/v). Samples were shaken for 20 h at 37 °C, then, the gels were rinsed with ultrapure water, frozen at -80 °C and lyophilized. Afterwards, samples were transferred to the metal supports and coated with a gold nanolayer and additionally sputtered with 5-nm-thick layer of Ti with an SPI sputter coater. All SEM images were obtained on SEM EVO LS15 with EDX, Resolution: 1kv SE e W (Zeiss, Jena, Germany) and FESEM ULTRA-Plus, Resolution: 1 kV e WD (Zeiss, Jena, Germany).

3D surface and porosity

The topography of freshly prepared hydrogels was studied using a Wyko® NT1100 microscope (Bruker, Tucson, AZ) by non-contact White Light Optical Interferometry (WLOI) and Vertical Scanning Interferometry (VSI). The images were analyzed by Wyko Vision 32 analytical Software package (Bruker, Tucson, AZ). Images of the hydrogels were obtained using Optical Microscope DMS 300, at 50× objective lens and an intermediate ×0.5 to obtain a magnification of 25.6×, with a field of view of 241×183 μm^2 of the samples. At least three zoomed areas from these topographic images were analyzed.

Three-dimensional parameters of surface texture and roughness: arithmetic mean height (S_a), root mean squared height (S_q), maximum height (S_z), skewness (S_{sk}), and kurtosis (S_{ku}) represent the statistical distribution of height values and were calculated by standard equations according to International Standard ISO 25178-2. S_{sk} represents the degree of symmetry of the surface heights about the mean plane. The sign of S_{sk} indicates the preponderance of peaks (that is $S_{sk} > 0$) or valley structures ($S_{sk} < 0$). S_{ku} reflects the nature of the height distribution and, therefore, it is useful for indicating the presence of either peak or valley defects such as scratches. If the surface heights are normally distributed (a bell curve) then S_{ku} is equal 3.00. Surfaces composed of inordinately high peaks/deep valleys have $S_{ku} > 3.00$. $S_{ku} < 3.00$ indicates gradually varying surfaces.

Rheological behaviour of hydrogels

A Discovery Hybrid Rheometer (DHR-2, TA Instruments, New Castle, DE) with the standard steel parallel-plate geometry of 20 mm diameter and a Physica MCR 101 rheometer (Anton Paar, Graz, Austria) with a plate-plate geometry with a diameter of 25 mm and a constant gap of 0.5 mm were employed for the rheological measurements. The agreement between the results in the two devices was checked and achieved in both non-linear viscoelastic tests and oscillatory shear mode. Firstly, flow curves for HA-fibrin hydrogel were carried out with the aim to obtain the initial viscosities. Then, the methods employed were oscillatory time sweeps, strain sweeps, and frequency sweeps. Time sweep experiments were performed to monitor the *in situ* gelation of the blank and NCs loaded hydrogel samples. During these time sweeps, a torque of 0.9 μN·m and a frequency of 0.5 Hz were maintained for a maximum time of 30 min to account for the temporal evolution of the elastic or storage modulus G' and the viscous or shear loss modulus, G". Strain sweeps were applied to characterize and compare G'/G" ratios under the same physical conditions identifying the linear viscoelastic region in the strain range from 0.1% to 1,000% or until structure breakdown. These tests were set up holding the frequency at 0.1 Hz or 1 Hz to ensure the best measuring conditions of the rheometer. Moreover, hydrogels samples were also subjected to oscillatory frequency sweep experiments, performed at frequencies from 0.01 to 100 Hz considering obtained linear viscoelastic region profiles, to study the stability of three-dimensional crosslinked networks [33].

The measurements were performed in triplicate at 20 °C and/or 37 °C. The results were analyzed using a Trios Software for DHR-2 rheometer and Rheoplus Software for Physica MRC 101.

Simulated synovial fluid (SSF) preparation

SSF was reproduced following the protocol described by Margareth and Raimar [34] and contained 0.017 M NaCl, 0.0027 M KCl, 0.01 M Na_2HPO_4, 0.00176 M KH_2PO_4, 3 mg/mL HA (non-specified MW), pH 7.4. 1.5 MDa HA was selected as one of the high MW HAs of normal human synovial fluid (SF) capable to maintain its viscosity. SSF was used in the stability and drug release experiments.

***In vitro* DXM release studies from the gel to SSF**

In situ non-fortified HA-fibrin hydrogel with 30% DXM loaded NCs was formed in SSF in a 1:1.3 (v/v, selected to comply with *in vivo* model). Briefly, the mixture of hydrogel and NCs was included in different vials corresponding to different incubation time points. Then, SSF warmed to 37 °C, was added to the mixture and the system was maintained under horizontal shaking (300 rpm) along the experiment. Once formed, at different time intervals (from 0 to 72 h), until the complete gel degradation, 100 µL of the medium surrounding the gel were withdrawn and mixed with 300 µL of EtOH (1:3) to extract the released DXM. The amount of released DXM was determined by HPLC as described above.

Carrageenan-induced acute knee joint inflammation (synovitis) model

Rats with an average body weight 281 ± 9 g were randomly distributed in groups (**Table 2**). Animals were anesthetized by intra-peritoneal injection (300 µL) of a solution containing ketamine (75 mg/kg) and medetomidine (0.50 mg/kg) and thereafter the skin around the knee joints was shaved. The acute synovial inflammation of the rat knee was induced 1 h after the treatment by IA injection of a freshly prepared solution of carrageenan (50 µL, 3% w/v) in physiological saline (0.9% w/v NaCl), using 27G needles, into the right knee of rats according to the technique described elsewhere [35,36].

***In vivo* treatment**

Rats were distributed according to the tested treatments. One animal served as reference for a gel syringeability test (referred as 0, **Table 2**), receiving HA-fibrin *in situ* gel with 30% blank NCs without inflammation induction. A control sub-group of 3 animals was injected with saline (group I, **Table 2**), another sub-group of 3 animals was induced with carrageenan (group II, **Table 2**), acting as a disease control. One group of animals was injected with blank NCs, used as a vehicle control (group 1, **Table 2**). Second group received with Gal-3 inhibitor loaded NCs administered at the dose of 200 µg/kg (group 2, **Table 2**). Third group was treated with HA-fibrin *in situ* gel with 30% Gal-3 inhibitor loaded NCs at the dose of 55 µg/kg (group 3, **Table 2**). A reference animal, a saline control sub-group and groups 1-3 received an IA injection (100 µL) of tested materials using low dead space syringes 30G × 1/2" Omnican 50 (BBraun, Hessen, Germany). All the components were mixed in the syringe and instantly injected into the right knee. The left knee without injection was used as a control.

Table 2. Control and experimental animal groups with respective treatments.

Group	Number of animals	Carrageenan 3% (µL)	Gal-3i dose (µg/kg)	Tested treatments	Injected treatment volume (µL)
Controls sub-groups:					
0	1	-	-	Gel + 30% blank NCs (syringeability test)	100
I	3			Saline	
II	3	50	-	-	-
Experimental groups:					
1	6	50	-	Blank NCs	100
2	6		200	Gal-3i NCs	
3	6		55	Gel + 30% Gal-3i NCs	

Samples for the reference animal (entitled 0, **Table 2**) and the experimental group 3 (**Table 2**), consisted of HA-fibrin hydrogel with 30% of blank or Gal-3 inhibitor loaded NCs, respectively, were prepared as presented in **Table 3**.

Table 3. Composition of HA-fibrin hydrogel + 30% NCs used for *in vivo* experiments.

Composition	Final concentration	Volume (µL)
Fibrinogen	1.5 mg/mL	6
HAs mix 1:1 (1.5 MDa:700 kDa) in HEPES buffer, 10^{-3} M Ca^{2+}, pH 7.4	0.5%	62
Blank or Gal-3i NCs	30%	30
Thrombin *(added as a last component)*	2 NIH-U/mL	2
Total volume		**100**

At time 4 h after carrageenan injection (the peak of inflammation) 3 animals of each group were sacrificed by isoflurane inhalation and blood was collected by cardiac puncture. The other animals were kept for knee measurements at 6 and 24 h.

Knee swelling measurement

The diameter of each rat shaved knee (in mm) was measured by digital calliper (150 mm / 6" - 0.01 mm, Perel Tools), before treatment and 2, 4, 6 and 24 h after carrageenan injection. Before measurements, rats were additionally anaesthetized with inhaled isoflurane. Knee swelling was expressed as the change (Δ) in the knee diameter before (B) and after (A) the induction of inflammation (*equation 1*), and the percentage of increase in knee diameter (knee edema) of the right knee of each rat at each time point was calculated by the *equation 2*:

Knee swelling $\Delta = A - B$ (*equation 1*),
Percentage of increase $= (A - B)/B \times 100$ (*equation 2*).

Histopathology studies

The animal hind limbs were surgically cut at the level above the patella. All the hind limbs were fixed in 10% buffered formalin and decalcified with 10% formic acid before histopathological analysis. In order to evaluate the surroundings of the site of application, decalcified hind limbs were processed for embedding in paraffin wax by using routine protocol. Sections (5 µm thick) were stained with haematoxylin and eosin (H&E). The slides were examined using light microscopy at 40, 100, 400× magnification using an Olympus BX40 microscope coupled with an Olympus DP 10 camera (Olympus, Shinjuku, Tokyo, Japan). The images were obtained using the respective Olympus DP 10 camera software and edited with Microsoft Image Composite Editor. The histopathological appearance of tissues was compared for structure changes, edema and inflammatory cell infiltration (mononuclear and/or polymorphonuclear cells).

Statistical analysis

All the measurements at each experimental condition were carried out in triplicates and were expressed as mean ± standard deviation (SD). The *in vivo* data presented as mean ± standard error of mean (SEM) for *n* animals. Differences among the groups were analysed by one-way ANOVA followed by Uncorrected Fisher's LSD multiple comparison test, using the software GraphPad Prism Co., version 8.0, CA, USA. Values of *p* lower than 0.05 were considered statistically significant.

3. Results and Discussion

Development and characterization of drug-loaded HA NCs

With the aim of prolonging drug release in the joint cavity, we developed a drug delivery system composed of NCs dispersed in an *in situ* forming hydrogel. Nanoparticles are physical biocompatibility — they are not expected to induce mechanical cartilage damage — and they show good injectability through very fine needles [37]. However, very small nanoparticles (below 100 nm) [38,39] may diffuse across the cartilage extracellular matrix (especially particles < 60 nm) and be easily drained from the synovial cavity to the blood and lymphatic circulation [2,40,41]. Therefore, we hypothesized that an adequate particle size for IA drug delivery would be slightly larger than 100 nm.

First, we developed HA NCs bearing DXM as a model drug, and then this technology was applied to encapsulate a novel drug candidate, Gal-3i. For the NCs preparation we selected: i) olive oil, due to its anti-inflammatory properties [42] and capacity to solubilize DXM [43] and Gal-3i; ii) soy lecithin and oleylamine, as surfactants, in order to produce cationic nanoemulsions to which the HA could be attached [44,45]; iii) HA (700 kDa) as a shell polymer due to its anti-inflammatory responses [46] (**Figure 1A**).

Drug-loaded HA NCs, prepared using the simple solvent displacement technique [30] showed an average particle size of 135 ± 9 nm and 122 ± 11 nm (for DXM-loaded and Gal-3i-loaded NCs, respectively) and negative surface charge (**Table 4**). DXM was encapsulated in large amounts based on the dose reported for IA administration 1.2 mg/kg in rats [47], while Gal-3i was expected to be efficient at microgram scale doses [48].

The core-shell structure of the NCs and their spherical shape could be visualized by TEM (**Figure 1B** and **C**). TEM images revealed smaller particle size values compared to DLS data.

These results can be explained considering that TEM requires detection of NCs in a dry state, whereas DLS analyses NCs in aqueous suspension, measuring the hydrodynamic diameter [49].

Table 4. Physicochemical characterization of the blank and drug-loaded nanocapsules (NCs) (mean ± SD; n = 6). DXM: dexamethasone, Gal-3i: galectin-3 inhibitor; PDI: polydispersity index.

Type of NCs	Particle size (nm)	PDI	ζ-potential (mV)	Drug concentration (mg/mL)
Blank	121 ± 10	0.2	−30 ± 3	n/a
DXM-loaded	135 ± 9	0.2	−31 ± 5	5.60 ± 0.40
Gal-3i-loaded	122 ± 11	0.2	−29 ± 5	0.53 ± 0.05

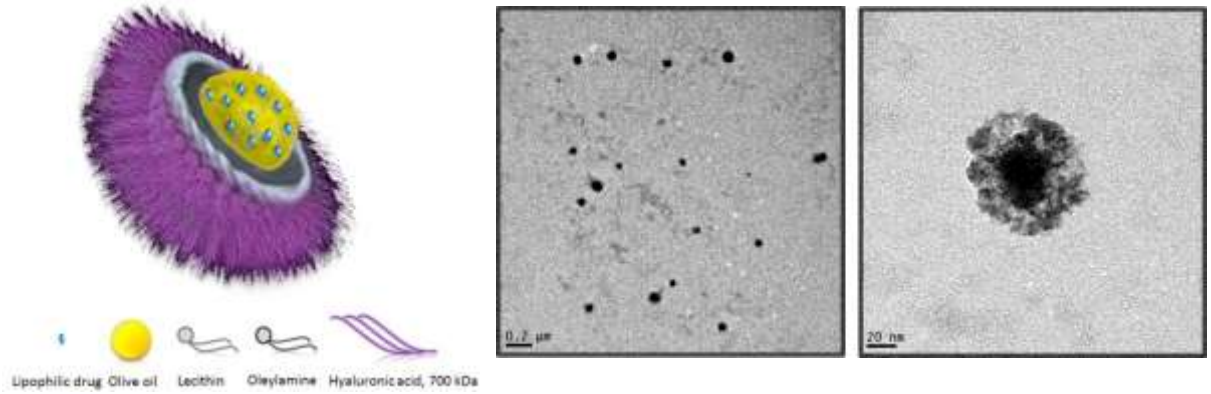

A **B** **C**

Figure 1. (A) Representation of the structure of drug-loaded hyaluronic acid (HA) nanocapsule (NC). TEM images of HA blank NCs: (**B**) at magnification 50,000×; (**C**) and 500,000×.

Development and characterization of *in situ* forming hydrogels

In order to increase the residence time of NCs in the articular cavity, we developed an *in situ* hydrogel composed of HA and fibrin, which in addition to having good rheological properties and high resistance to IA deformations, would serve as a reservoir for the NCs.

Fibrin, a biomaterial derived from human blood plasma, marketed as a glue sealant under the name of Tisseel® (Baxter Healthcare corporation, USA), was selected as a key component of the hydrogel [50]. Such combination of HA and fibrin has been previously used in tissue engineering (TE) [51,52]. Moreover, RegenoGel®, composed of fibrinogen chemically linked to a high MW HA, has been recently marketed in Israel as a medical device indicated for the treatment of OA [53]. On the other hand, HA, being a key component of articular cartilage and SF, and having an essential role in diarthrodial joints homeostasis [54,55], was selected as a biomaterial to form the hydrogel. HA was also expected to improve joint lubrication and have a chondroprotective effect [55,56]. Besides, HA has been reported to have anti-inflammatory and antinociceptive properties [55,57].

In a first step we developed a hydrogel based on thrombin-induced conversion of fibrinogen to fibrin 3D network (**Table 5**). In these experiments thrombin was used at various concentrations (0.1-2 NIH-U/mL). In the first stage of polymerization, shown as the "fluid" phase in **Figure 2A**, fibrin is presented in the form of soluble fibrin-monomers. The second stage of polymerization [58] is characterized by the lateral association of protofibrils to fibrils and their subsequent organization in a 3D-network hydrogel (**Figure 2C**) [50,59]. This process is characterized by a constant increase of the absorbance until the gel is completely formed (the "gel" phase, **Figure 2A**). The time at which fibrin starts to polymerize (gelation point) was calculated from the kinetics curves of polymerization by the method described by Chernysh *et al.* [59] (**Figure 2B**). The results presented in **Figure 2A** and **B** indicate that the optimal gelation rate at physiological conditions was achieved with a thrombin concentration in the range of 1-5 NIH-U/mL [58].

In the following step, taking advantage of the affinity between HA and fibrin's positively charged E- and αC-domains ($K_d \sim 45 \times 10^{-9}$ M) [60,61], we explored the formation of HA-fibrin hydrogels. HA of different MW (40 kDa, 700 kDa, and 1.5 MDa) in various concentrations were used. The gelation point of the HA-fibrin system was calculated from the kinetics curves of polymerization, as described above for fibrin kinetics. For these experiments, 0.1%, 0.25%, and 0.5% (w/v) solutions of HA of each MW (40 kDa, 700 kDa and 1.5 MDa) and a mixture of 700 kDa and 1.5 MDa were used (**Table 5**). Beyond that, the concentration of Ca^{2+} ions in HA solutions, similar to the one found in plasma ($1\text{-}1.1\times10^{-3}$ M) [58], was expected to modulate the speed of polymerization, gel rheology, and porosity.

Table 5. Screening of compositions to optimize HA-fibrin gel formation. Fg: fibrinogen, Thr: Thrombin, HA: hyaluronic acid, FXIII: factor XIII, α2AP: α2-antiplasmin, MW: molecular weight.

System	**Components concentrations**					
	Fg (mg/mL)	**Thr (NIH-U/mL)**	**HA**		**FXIII (µg/mL)**	**α2AP (µg/mL)**
			w/v	**MW**		
Fibrin gel	1	0.1 - 2	-	-	-	-
HA-fibrin gel	1	0.5 - 1	0.1 - 0.5%	40 kDa	-	-
			0.1 - 0.5%	700 kDa		
			0.1 - 0.5%	1.5 MDa		
			0.5%	Mix 1:1 of 700 kDa : 1.5 MDa		
Fortified HA-fibrin gel	1	0.75 - 1	0.5%	Mix 1:1 of 700 kDa : 1.5 MDa	10	0.14

As shown in **Figure 2D**, the higher the concentration and MW of HA the higher the inhibition degree of the gelation process. However, in the case of 40 kDa HA, due to the low MW, the influence of the HA concentration had only a minor impact on the gelation process. On the other hand, 0.5% 1.5 MDa HA solution was highly viscous and, thus, difficult to inject. As a compromise, a mixture of HAs (700 kDa:1.5 MDa = 1:1, 0.5%), with moderate viscosity, was selected to modulate the gelation time and enable adequate syringeability. This composition

was previously reported to be good for viscosupplementation purposes [62]. Furthermore, HA with a MW of 0.5-1 MDa has been found to be effective in reducing synovial inflammation [18,57], while 1.3-1.7 MDa HAs are able to restore the rheological properties of arthritic synovial fluid [46,63]. The total amount of HA, both endogenous and exogenous, reaching the synovial cavity *in vivo* with this formulation, was estimated to be ~3 mg/mL, which corresponds to its physiological concentration in healthy SF [64].

Finally, two fortifying agents were added to the system in order to reduce the degradation time of the HA-fibrin hydrogel: FXIII and α2AP. FXIII is a natural fibrin covalent crosslinker that fortifies and stabilizes the fibrin mesh, increasing the resistance of the gel against degradation [65,66]. Simultaneously, α2AP, was expected to reduce the degradation of crosslinked fibrin gels by plasmin [67], a component normally found in rheumatic SF [68].

Hence, by adding FXIII and α2AP to *in situ* HA-fibrin hydrogel a fortified HA-fibrin interpenetrating polymer network was engineered (**Figure 2C**). This combination of materials is expected to hamper the action of hyaluronidase, which quickly degrades non-crosslinked HA in inflammatory joint diseases [69]. The influence of FXIII and α2AP on the hydrogel formation was analyzed by turbidity analysis. The results indicate that, as expected, the gelation time is reduced upon addition of FXIII, also confirmed by rheology data (**Figure 2E**).

Overall, we were able to control the polymerization rate and the rheological properties of the developed hydrogel by adjusting different parameters, namely the amount of thrombin, the MW and concentration of HA, Ca^{2+}, and FXIII.

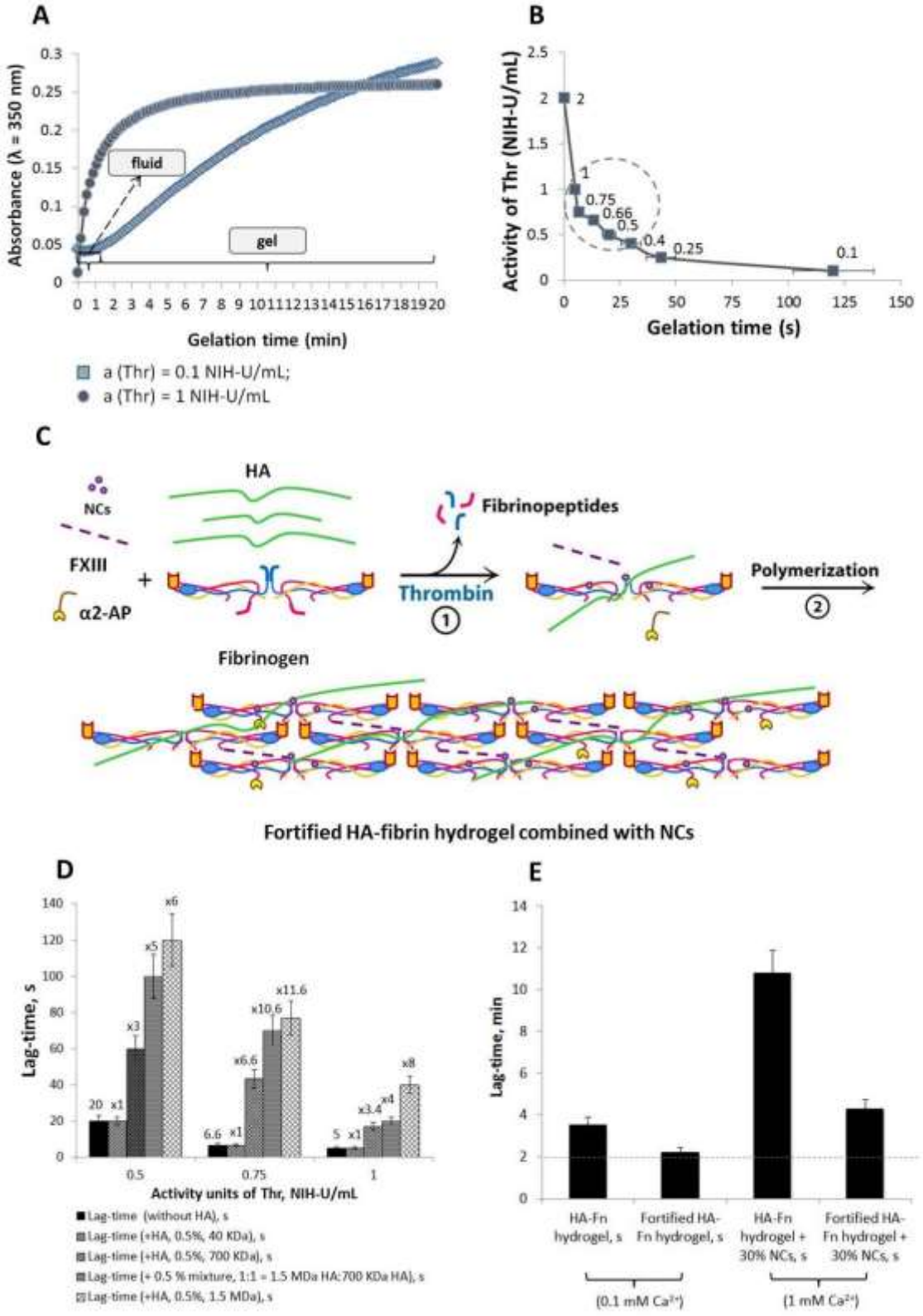

Figure 2. A stepwise development of the *in situ* hydrogel based on thrombin-induced conversion of fibrinogen to fibrin 3D network. The influence of thrombin (Thr) on the fibrin (Fn) gelation profile **(A)**: at activity 0.1 and 1 NIH-U/mL, and **(B)** the gelation times at activity 0.1 - 2 NIH-U/mL. The range marked by dot-dash line circle represents the Thr activity at which the hydrogels showed the best stability profiles over time. The

polymerization kinetics was determined by turbidity analysis during 20 min at λ = 350 nm. Fibrinogen = 1 mg/mL; Thr, 1 NIH-U = 0.324 ± 0.073 μg (9.0 nM). **(C)** The schematic illustration of the fortified HA-fibrin gel formation, activated by Thr, in the presence of nanocapsules (NCs). **(D)** Influence of HA MW on fibrin polymerization kinetics. **(E)** Gelation time points determined by rheological measurements in different systems: HA-fibrin and fortified HA-fibrin blank and 30% NCs loaded gels. For blank gels, fibrinogen was always taken at 1 mg/mL concentration, activity of thrombin (Thr) = 1 NIH-U/mL. For 30% NCs loaded gels, fibrinogen was always taken at 1.5 mg/mL concentration, activity of Thr = 2 NIH-U/mL. The dot-dash line reflects the required 2 min lag-phase. All the measurements were carried out at 37 °C. Expressed as mean ± SD; *n* = 3. Fn: fibrin, Thr: thrombin, HA: hyaluronic acid, FXIII: factor XIII, α2AP: α2-antiplasmin.

NCs loading into the hydrogels

We investigated the capacity of the hydrogels (fortified and non-fortified) to load NCs in the range of 10 – 50% (v/v) (**Table 1**). NCs showed a significant inhibition of the gel formation process (> 20 min) and no gelation was observed when the NCs/hydrogel v/v ratio was higher than 30%. Based on this information, the next step was to adjust the formulation conditions (fibrin, thrombin, Ca^{2+} and HAs concentrations) to achieve a 30% NCs loaded hydrogels.

In order to reach an adequate syringeability of *in situ* hydrogel for *in vivo* experiments, our approach was to delay the gel formation for at least a 2 min lag-time after mixing the gel components. The optimal gelation time for the formation of a HA-fibrin hydrogel with adequate rheological properties (marked with a dot-dash line in **Figure 2E**) was achieved at a concentration of 1.5 mg/mL fibrinogen, 2 NIH-U/mL thrombin, 0.5% (w/v) mixture 700 kDa:1.5 MDa HAs and 10^{-3} M Ca^{2+}. In the case of the fortified HA-fibrin hydrogel, 10 μg/mL of FXIII and 0.14 μg/mL α2AP were additionally added. **Figure 2E** shows a summary of the polymerization kinetics observed by rheological measurements.

Rheological behaviour of the hydrogels containing NCs

A basic requirement for the development of an *in situ* gelling system is that it has a low vicosity in order to ensure a good syringeability. The viscosity of the HA-fibrin mixture (before the gelation) at 20 °C and 37 °C is 118.9 mPa·s and 81.3 mPa·s, respectively. These values are much lower than those of commercial viscosupplements [70]. Thus, mixed solutions designed to form the *in situ* hydrogel are expected to be easily injected intra-articularly.

Oscillatory rheological experiments are a useful tool to determine the macro- and micro-structural rearrangements that influence the rheological behaviour of gels over time [71]. The gelling point can be detected by monitoring the gelation process with an oscillatory time sweep. The temporal evolution of the elastic or storage modulus (G'), which measures the elastic nature of the material, and the viscous or shear loss modulus (G"), which measures the viscous nature of the material, was monitored upon the tests. **Figure 3A** and **B** shows the gelation process of HA-fibrin and fortified HA-fibrin hydrogels with 30% loaded NCs. Initially, G" is higher than G', due to the liquid state of the samples, where the viscous properties predominate. As soon as the hydrogels begin to form a crosslinked network the two indicated moduli rise. Nevertheless, the increase of G' is faster than that of G", because the elastic nature of the gelling system starts to dominate. Hence, a crossover point appears in the curves corresponding to the gelation time of the sample. The time frame until the crossover point represents the lag-time. The gelation times of HA-fibrin and fortified HA-fibrin blank gels are shown in **Figure 2E**). As noted in these figures, the gelation time decreases significantly in the fortified HA-fibrin hydrogels. As

observed in both the rheological and turbidity assays, the incorporation of NCs led to an increase in the gelation time of the system.

The deformation profiles of the hydrogels were measured by analysing the G' and G" moduli using an oscillatory strain and frequency sweeps. As an example, **Figure 3C and D** shows the elastic and viscous moduli evolution of the non-fortified and fortified HA-fibrin hydrogels loaded with 30% NCs as a function of the increasing deformation. Initially, linear viscoelastic region, i.e. the region in which stresses are not large enough to irreversibly deform the material structure, was identified through deformation sweeps in which the strain was logarithmically increased from 0.1% to 1,000% or 10,000%, depending on the parameters of the G'=G" crossover point. At strains lower than 10-15% (critical strain), the value of elastic and viscous moduli was constant and independent of the deformation. In the linear viscoelastic region presented in **Figure 3C and D** the deformation was completely recoverable and the material exhibits an elastic "solid-like" behaviour, G' > G". This was expected as HA and fibrin are supposed to have a synergistic effect and provide the hydrogel with improved mechanical properties and resistance against deformations [72,73]. Indeed, it has been reported that the high hydrophilicity of HA prevents the compression of the fibrin network and improves its mechanical properties [73], while fibrin provides the hydrogel with the desired elasticity and resistance [74].

The crossover point of G' and G" moduli, indicative of sample destruction, was observed at strains of 630% and 100% for the fortified and non-fortified HA-fibrin gels containing NCs. Thus, NCs-loaded fortified gels were 6.3 times more resistant to deformations than the non-fortified gels. Other authors also showed that fibrin hydrogels crosslinked by FXIII under physiological conditions were more stable and exhibited 8 times higher Young's (elastic) modulus values than non-crosslinked hydrogels [74].

For deformations occurring around strain 100% an "overshoot phenomenon" was observed in the G' and G" moduli of the fortified HA-fibrin hydrogel loaded with 30% NCs (**Figure 3D**). This response is typical for materials with resistance to a permanent deformation, which is evidence of the FXIII contribution to the stability profile in terms of rigidity and strength. Lorand *et al.* also observed an increase in viscous and elastic moduli of fibrin gel crosslinked by FXIII as a measure of hydrogel stability against shear stress [66]. At the higher strains applied, the values of two moduli decreased as the strain increased corresponding to thinning behaviour previous to the breakdown of the material structure.

The oscillatory frequency sweeps exhibited a plateau-type behaviour of the G' and G" modulus in the range 0.01-1 Hz for 30% NCs loaded non-fortified and fortified HA-fibrin gels (Supporting Information, **Figure S1**), which is indicative of a stable crosslinked network. In all cases the hydrogel samples showed an increase in G' at higher frequencies assuming "solid-like" behaviour characterized by an increase of the elastic modulus. Interestingly, hydrogels containing NCs showed higher stability against deformations than blank gels and, thus, longer persistence. This observation could be explained on the basis of ionic interactions between the NC's HA shell and the fibrin present in the hydrogel [61,75].

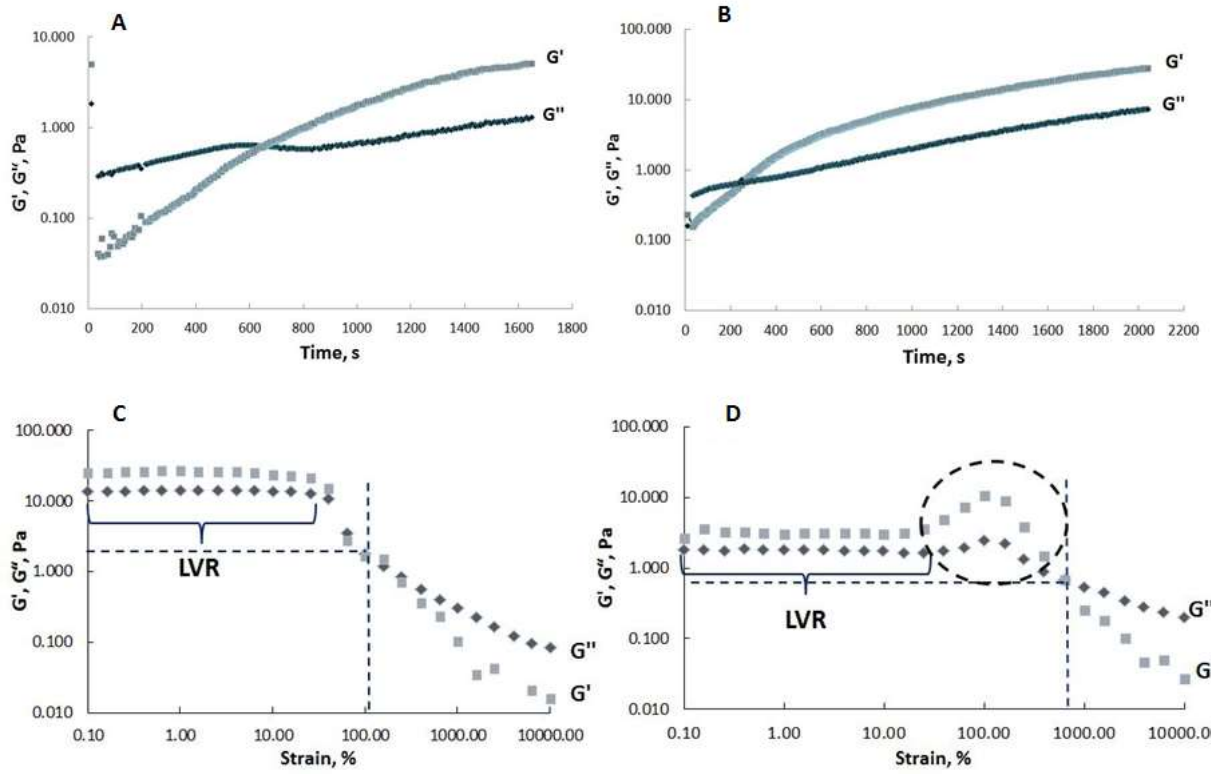

Figure 3. (A) Gelation point detection by the response of elastic (G') and viscous (G'') moduli in non-fortified HA-fibrin and **(B)** fortified HA-fibrin hydrogels loaded with NCs (30%). **(C)** Deformation point detection measured by the response of elastic (G') and viscous (G'') moduli in HA-fibrin and **(D)** fortified HA-fibrin systems with 30% loaded NCs, as a function of strain at 1 Hz. Linear viscoelastic region is denoted as LVR. The area marked by the circle represents an overshoot phenomenon. Fibrinogen concentration was 1.5 mg/mL, activity of thrombin = 2 NIH-U/mL. The measurements were carried out at 37 °C. Expressed as mean ± SD; $n = 3$.

Overall, these results indicate the posibility to engineer HA NC-containing hydrogels composed of HA and fibrin, crosslinked with FXIII, with the adequate mechanical and elastic properties for IA application *in vivo*.

Surface morphology and porosity of *in situ* forming hydrogels

The topographic characterization of HA-fibrin and fortified HA-fibrin loaded with 30% of NCs was performed (Supporting Information, **Table S1**). As an example, the topography of the blank and NCs loaded non- and fortified HA-fibrin hydrogels is shown in **Figure 4A, D, G, J**. These hydrogels have a homogenous structure with normally distributed surface heights and valleys and a well-organized porous architecture. The average pore sizes for HA-fibrin and fortified HA-fibrin hydrogels are summarized in **Table S2**. Fortified HA-fibrin hydrogels containing NCs have a smaller pore size (4.88 ± 1.12 μm) than the non-fortified ones loaded with NCs (7.29 ± 1.23 μm). These measurements correlate well with the data obtained from SEM.

Liquid compositions of *in situ* hydrogels, injected through a fine insulin needle (29G) to the vials, were incubated for 20 h at 37 ºC to allow the formation of mature hydrogels, which were then lyophilized and analyzed by SEM and FESEM (**Figure 4B, C, E, F, H, I, K, L, N, O**). The images shown below confirmed that fortified HA-fibrin gels had more compact structure

than the non-fortified ones. In addition, microscopy images show fibrin gel fibrils of 1-2 μm in diameter (**Figure 4N, O**), such fibril thickness is a feature of stable fibrin hydrogels [58].

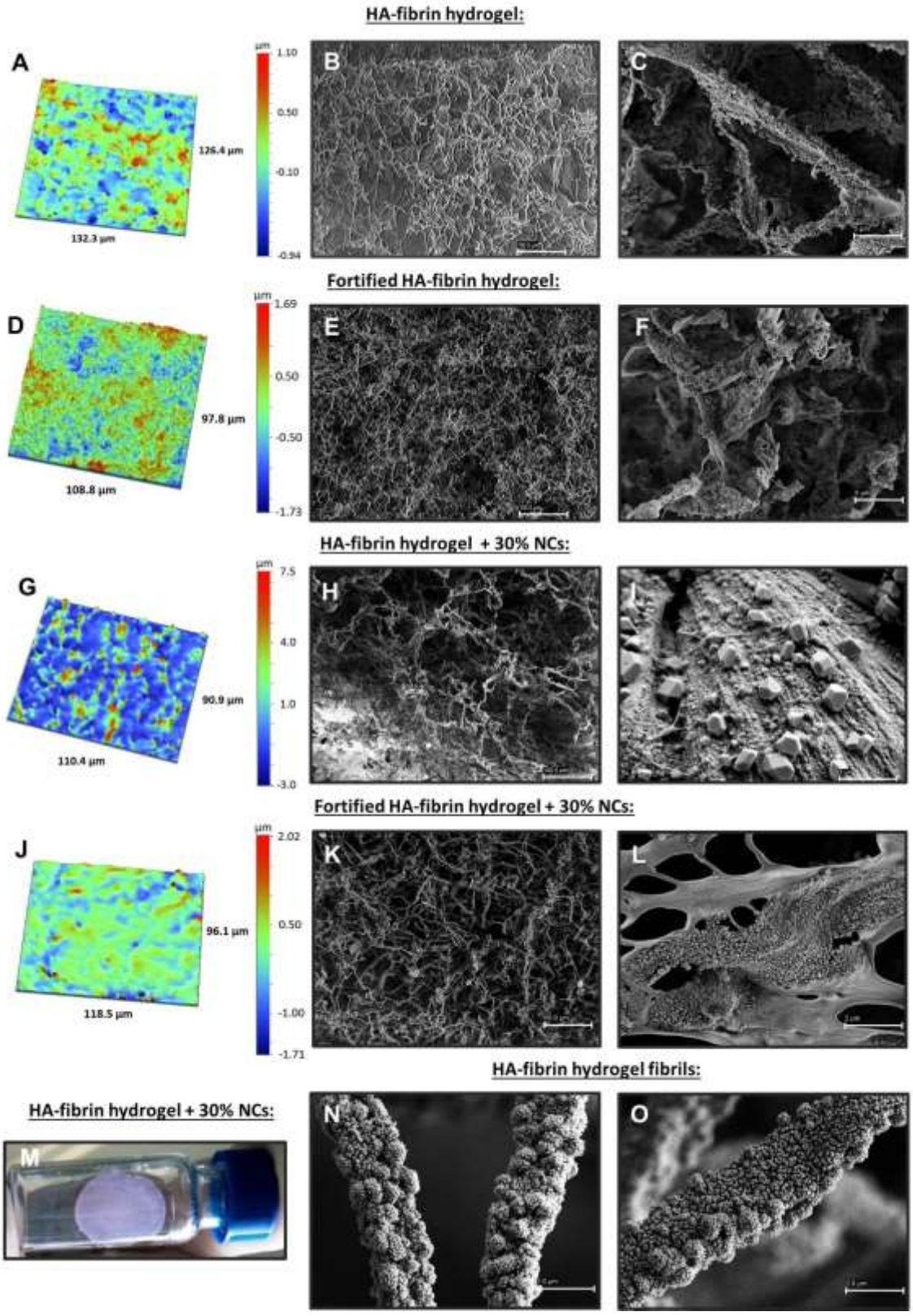

Figure 4. A vertical raw of 3D topographical images represents **(A)** HA-fibrin hydrogel, **(D)** fortified HA-fibrin hydrogel, **(G)** HA-fibrin hydrogel + 30% NCs, and **(J)** fortified HA-fibrin hydrogel + 30% NCs, obtained with the spatial resolution of the optical profiler. Red

color represents surface peaks, blue represents valleys. SEM images of **(B)** HA-fibrin and **(E)** fortified HA-fibrin hydrogels at magnification 500×. FESEM images of **(C)** blank HA-fibrin and **(F)** blank fortified HA-fibrin hydrogels at magnification 10,000×. FESEM images of **(H)** HA-fibrin hydrogel + 30% NCs at magnification 500× and **(I)** at magnification 30,000×, **(K)** fortified HA-fibrin hydrogel + 30% NCs at magnification 1000×, and **(L)** at magnification 30,000×. **(M)** Nile Red-labelled NCs dispersed in the HA-fibrin hydrogel (30% loading). FESEM images of **(N, O)** HA-fibrin hydrogel at magnification 30,000×.

In vitro drug release from NCs loaded hydrogels

The release studies of the model drug (DXM) were carried out under sink conditions in SSF at 37 ºC for both, NCs and NCs-loaded non-fortified HA-fibrin hydrogels. 70% of the drug was released from the free NCs in a burst manner in the first hour of incubation; a 100% release was attained in 24 h *(data not shown)*. In contrast, in the case of NCs loaded non-fortified HA-fibrin hydrogel a slow release was observed in SSF (Supporting Information, **Figure S2**). More precisely, ~30% of the model drug (DXM) was released in the first time point, followed by a slow release of up to ~50% within 24 h. In the next 24-60 h, up to the 60% of the drug was released gradually. Between 60-72 h, the gel started to slowly degrade, and a 100% release of the model drug was reached at 72 h. Overall, these results underline the importance of the hydrogel in controlling the release of the drug.

These *in vitro* release results are in line with other previously reported in the literature [76,77]. However, there are other works reporting a much more prolonged release. Namely, Webber *et al.* showed the possibility to control the release for up to 32 days upon conjugation of DXM to a peptide-based nanofiber gels [78]. Similarly, Wu *et al.* disclosed the possibility to prolong the *in vitro* release of DXM from micelles loaded into a PEG-PCL-PEG hydrogel for up to one month [4]. In this work, we studied the non-fortified hydrogels in order to have preliminary information regarding the controlled release behaviour of the system. However, we have speculated that the release from the NCs-loaded fortified HA-fibrin hydrogel would be more prolonged, as the degradation rate of the hydrogel would be retarded due to FXIII and α2-antiplasmin enzyme in the composition [79]. Irrespective of the crosslinking degree, there is the possibility that the release of DXM occurred by a simple diffusion process and was not controlled by the degradation of the hydrogel. In any case, the interpretation of these data should be cautiously done, as the *in vitro* release conditions are very different from the ones found in an *in vivo*.

Loading of Gal-3 inhibitor into HA NCs and subsequent incorporation into a HA-fibrin hydrogel

After the optimization of the hydrogels with a model anti-inflammatory drug (DXM), a carbohydrate-based small molecule Gal-3i (2-azidoethyl [3-*O*-(2-naphtyl)methyl-β-D-galactopyranosyl]-(1-4)-2-deoxy-2-(3-methoxybezamido)-β-D-glucopyra-noside) [26,27] was encapsulated in the developed drug delivery system for the evaluation of Gal-3 inhibition *in vivo*. The extracellular protein Gal-3 was recently identified as a primer trigger of the pro-inflammatory cascade in arthritis [28,29]. Noticeably, Gal-3 expression is up-regulated in synovial tissues in RA and OA [80], its concentration in SF increases from about 50 up to 130-300 ng/mL [29]. This protein favours the secretion of macrophage pro-inflammatory cytokines, chemokines [29], and matrix metalloproteinases [68], which are involved in cartilage remodeling and bone demineralization [81]. Currently, three Gal-3 antagonists have entered clinical trials for the treatment of different pathologies [82,83], however, none of them was intended for joint diseases treatment.

***In vivo* study of the anti-inflammatory activity of Gal-3 inhibitor loaded in a NCs-containing hydrogel**

Acute inflammatory rat models (induced by carrageenan 0.6-3% solutions) [36,42] share similar features with human RA and constitute a useful tool for drug screening and designing specific therapeutic interventions in order to suppress synovial inflammation [84]. As any inflammatory model, it expresses galectin-3 (>95.5% homology between human and rat Gal-3 carbohydrate recognition domains) [85,86], which makes the rat models appropriate for *in vivo* testing of human Gal-3 inhibitors [29].

The non-fortified HA-fibrin hydrogel loaded with 30% NCs was considered to be adequate for short-term release in an acute knee joint synovitis model.

The IA injection of carrageenan led to a significant increase of the knee diameter of the hind limb (~ 40%), in comparison to the saline injection [36]. As shown in **Figure 5,** the increase in the knee diameter was gradual and reached a significant value at 4 h after carrageenan injection (close to 4 mm increase in the diameter). Interestingly, this increase was significantly lower for the groups of animals treated with Gal-3i-loaded NCs and non-fortified Gal-3i-loaded HA-fibrin hydrogel (Gel, **Figure 5**). More specifically, Gal-3i NCs at the dose of 200 µg/kg reduced the inflammation in about 3.3 times at 4 h compared to carrageenan control, whereas the effective swelling inhibition achieved with the HA-fibrin hydrogel with 30% Gal-3i NCs was 7.4 times lower compared to the carrageenan control. It is important to highlight that this effective swelling reduction was achieved using a low dose of Gal-3i (55 µg/kg). Considering that there was no previous information about the effectiveness of this Gal-3 inhibitor for IA application, the rationale behind this dose was to use the maximum feasible concentration of the drug, so with the NCs-loaded hydrogel we could only test around 30% of the dose tested in the NCs. Our hypothesis is that HA-fibrin hydrogel effectively keeps NCs within the articular cavity, modulating the drug release and, by itself, showing a beneficial effect on joints healing.

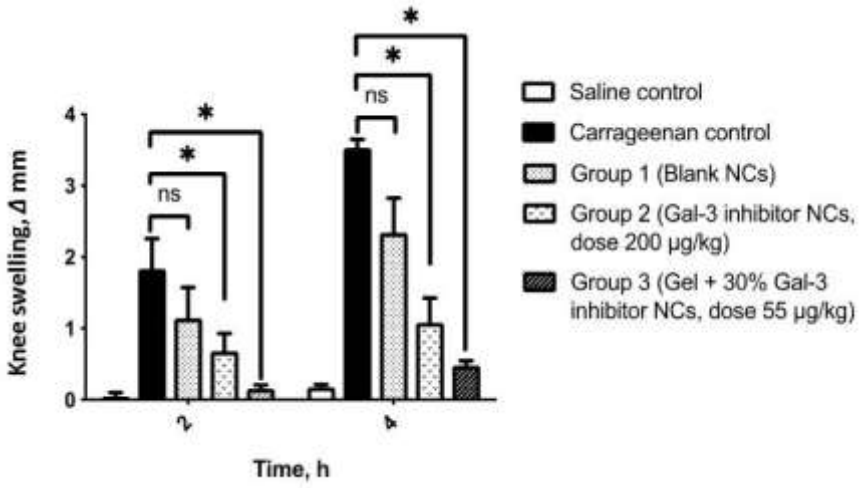

Figure 5. Effect of the treatment with Gal-3 inhibitor on the carrageenan-induced joint inflammation model using nanocapsules (NCs), and NCs in HA-fibrin hydrogel compared to blank NCs ($n = 6$), carrageenan and saline control ($n = 3$). Δ is the difference in knee diameter at various time points before and after injection of carrageenan, expressed in mm. Data is expressed as mean ± SEM, * $p < 0.05$ versus carrageenan control.

Histopathological analysis was used as a tool to visualize changes in rat knee joints. After the decalcification process the rat hind limbs and knees were sliced, stained and analyzed by light microscopy (Supporting Information, **Figure S3**). As expected, none of the drug delivery system components caused an inflammatory response *in vivo*. Cirino *et al*. found that intra-articularly administered thrombin mediates inflammation in the rat hindpaw at doses of 1-10 NIH-U/limb [87]. In our study, the hydrogel formation was activated by thrombin at 0.2 NIH-U per injection; 5 times lower than the limit causing moderate inflammation. The formulation Gel + blank NCs, injected alone, presented neither microscopic articular cartilage nor synovial membrane changes. Besides, articular cavity was free of neutrophils and no sign of cell infiltration was detected in the surrounding tissues (Supporting Information, **Figure S3D**), suggesting that the drug delivery system is well-tolerated *in vivo*.

The improvement at the histological level was gradually observed from carrageenan control to group 3, suggesting that Gal-3i in its final drug delivery system (Gel + 30% NCs) had the most detectable impact on the inhibition of synovial inflammation and the articular tissues integrity in the acute synovitis rat model (Supporting Information, **Figure S3**). Group 3 had less synovial membrane changes than other groups, besides, the articular cavity was free of neutrophils and no signs of cell infiltration were detected in the surrounding tissues.

Simultaneously, this study provides the insights of a preliminary unprecedented *in vivo* evaluation of the Gal-3i effects in the acute synovitis rat model. More tests are required to understand the Gal-3i behaviour and its impact on the course of the inflammatory joint diseases *in vivo*.

4. Conclusions

Here, we report a new nanotechnology-based delivery system and its potential IA treatment of inflammatory joint diseases. The system consists of an injectable in situ hydrogel made of HA and fibrin combined with HA NCs, loaded with lipophilic anti-inflammatory drugs. The rheological properties of the system enabled a good syringeability and desirable mechanical properties for IA application. The results obtained in a preliminary in vivo acute knee synovitis rat model show a remarkable suppression of inflammation by Gal-3 inhibitor encapsulated within NCs loaded in an in situ hydrogel and administrated intra-articularly. These findings suggest this system may represent a strategy to alleviate the inflammatory conditions of large joints. However, further studies are required to explore this tool for tissue engineering in chronic models of synovial inflammation. At the same time, future efforts will be focused on the optimisation of the drug release kinetics from the hydrogel by modifying the parameters that influence the gelation properties (e.g. concentration of HA, fibrin, crosslinkers and a NCs loading rate).

Supporting Information

Supporting Information is available from the authors.

Acknowledgements The authors express gratitude for financial support from EM NanoFar Doctoral Fellowship (Project 2013-05-C2-EM), Xunta de Galicia (Competitive Reference Groups-FEDER Funds Ref: ED431C 2017/09, ENE2017-86425-C2-1-R Project), Xunta de Galicia and the Laboratoires Servier for post-doctoral fellowships, and Fundação para a Ciência e a Tecnologia (Program UID/DTP/04138/2013).

Conflict of Interest

The authors declare no conflict of interest.

Compliance with Ethical Standards

All institutional and national guidelines for the care and use of laboratory animals were followed.

References

1. Evans CH, Kraus VB, Setton. LA. Progress in intra-articular therapy. Nat Rev Rheumatol. Nature Publishing Group; 2015;10:11–22.

2. Burt HM, Tsallas A, Gilchrist S, Liang LS. Intra-articular drug delivery systems: Overcoming the shortcomings of joint disease therapy. Expert Opin Drug Deliv. 2009;6:17–26.

3. Kang ML, Im G-I. Drug delivery systems for intra-articular treatment of osteoarthritis. Expert Opin Drug Deliv. 2014;11:269–82.

4. Wu Q, Wang N, He T, Shang J, Li L, Song L, et al. Thermosensitive hydrogel containing dexamethasone micelles for preventing postsurgical adhesion in a repeated-injury model. Sci Rep. 2015;5:13553.

5. Ho MJ, Kim SR, Choi YW, Kang MJ. Recent advances in intra-articular drug delivery systems to extend drug retention in joint. J Pharm Investig. 2018;49:9–15.

6. Van Den Hoven JM, Van Tomme SR, Metselaar JM, Nuijen B, Beijnen JH, Storm G. Liposomal drug formulations in the treatment of rheumatoid arthritis. Mol Pharm. 2011;8:1002–15.

7. Kapoor B, Singh SK, Gulati M, Gupta R, Vaidya Y. Application of liposomes in treatment of rheumatoid arthritis: Quo vadis. Sci World J. 2014;2014.

8. Sarkar A, Carvalho E, D'Souza AA, Banerjee R. Liposome-encapsulated fish oil protein-tagged gold nanoparticles for intra-articular therapy in osteoarthritis. Nanomedicine. 2019;14:871–87.

9. Huang G, Zhang Z. Micro- and nano-carrier mediated intra-articular drug delivery systems for the treatment of osteoarthritis. J Nanotechnol. 2012;2012.

10. Yang M, Feng X, Ding J, Chang F, Chen X. Nanotherapeutics relieve rheumatoid arthritis. J Control Release. 2017;252:108–24.

11. Bartneck M, Peters FM, Warzecha KT, Bienert M, van Bloois L, Trautwein C, et al. Liposomal encapsulation of dexamethasone modulates cytotoxicity, inflammatory cytokine response, and migratory properties of primary human macrophages. Nanomedicine Nanotechnology, Biol Med. 2014;10:1209–20.

12. Hofkens W, Schelbergen R, Storm G, van den Berg WB, van Lent PL. Liposomal Targeting of Prednisolone Phosphate to Synovial Lining Macrophages during Experimental Arthritis Inhibits M1 Activation but Does Not Favor M2 Differentiation. PLoS One. 2013;8:1–11.

13. Kang ML, Kim JE, Im G Il. Thermoresponsive nanospheres with independent dual drug release profiles for the treatment of osteoarthritis. Acta Biomater. 2016;39:65–78.

14. Ye J, Wang Q, Zhou X, Zhang N. Injectable actarit-loaded solid lipid nanoparticles as passive targeting therapeutic agents for rheumatoid arthritis. Int J Pharm. 2008;352:273–9.

15. Bajpayee AG, Grodzinsky AJ. Cartilage-targeting drug delivery: can electrostatic interactions help? Nat Rev Rheumatol. 2017;13:183–93.

16. Bias P, Labrenz R, Rose P. Sustained-release dexamethasone palmitate: Pharmacokinetics

and efficacy in patients with activated inflammatory osteoarthritis of the knee. Clin Drug Investig. 2001;21:429–36.

17. Paik J, Duggan ST, Keam SJ. Triamcinolone Acetonide Extended-Release: A Review in Osteoarthritis Pain of the Knee. Drugs. 2019;79:455–62.

18. Goldberg VM, Goldberg L. Intra-articular hyaluronans: the treatment of knee pain in osteoarthritis. J Pain Res. 2010;3:51–6.

19. Strauss EJ, Hart J a, Miller MD, Altman RD, Rosen JE. Hyaluronic Acid Viscosupplementation and Osteoarthritis. Am J Sports Med. 2009;37:1636–44.

20. Zhang Z, Wei X, Gao J, Zhao Y, Zhao Y, Guo L, et al. Intra-articular injection of cross-linked hyaluronic acid-dexamethasone hydrogel attenuates osteoarthritis: An experimental study in a rat model of osteoarthritis. Int J Mol Sci. 2016;17.

21. Rutjes AWS, Ju P, Costa BR, Trelle S, Nu E. Annals of Internal Medicine Viscosupplementation for Osteoarthritis of the Knee. Ann Intern Med. 2012;157:180–91.

22. Petit A, Redout EM, van de Lest CH, de Grauw JC, Müller B, Meyboom R, et al. Sustained intra-articular release of celecoxib from in situ forming gels made of acetyl-capped PCLA-PEG-PCLA triblock copolymers in horses. Biomaterials. 2015;53:426–36.

23. Turker S, Ozer a Y, Kilic E, Ozalp M, Colak S, Korkmaz M. Gamma-irradiated liposome/noisome and lipogelosome/niogelosome formulations for the treatment of rheumatoid arthritis. Interv Med Appl Sci. 2013;5:60–9.

24. Lei Y, Rahim M, Ng Q, Segura T. Hyaluronic acid and fibrin hydrogels with concentrated DNA/PEI polyplexes for local gene delivery. J Control Release. 2011;153:255–61.

25. Liu M, Zeng X, Ma C, Yi H, Ali Z, Mou X, et al. Injectable hydrogels for cartilage and bone tissue engineering. Bone Res. 2017;5:17014.

26. Dion J, Deshayes F, Storozhylova N, Advedissian T, Lambert A, Viguier M, et al. Lactosamine-Based Derivatives as Tools to Delineate the Biological Functions of Galectins: Application to Skin Tissue Repair. ChemBioChem. 2017;18:782–9.

27. Coppin L, Vincent A, Frénois F, Duchêne B, Lahdaoui F, Stechly L, et al. Galectin-3 is a non-classic RNA binding protein that stabilizes the mucin MUC4 mRNA in the cytoplasm of cancer cells. Sci Rep. 2017;7:43927.

28. Janelle-Montcalm A, Boileau C, Poirier F, Pelletier J-P, Guévremont M, Duval N, et al. Extracellular localization of galectin-3 has a deleterious role in joint tissues. Arthritis Res Ther. 2007;9:R20.

29. Hu Y, Yéléhé-Okouma M, Ea HK, Jouzeau JY, Reboul P. Galectin-3: A key player in arthritis. Jt Bone Spine. 2017;84:15–20.

30. Crecente-Campo J, Alonso MJ. Engineering, on-demand manufacturing, and scaling-up of polymeric nanocapsules. Bioeng Transl Med. 2018;4:38–50.

31. Urban CMC, Mainardes RM, Gremião MPD. Development and validation of HPLC method for analysis of dexamethasone acetate in microemulsions. 2009;45.

32. Kupper CE, Rosencrantz RR, Henßen B, Pelantová H, Thönes S, Drozdová A, et al. Chemo-enzymatic modification of poly-N-acetyllactosamine (LacNAc) oligomers and N,N-diacetyllactosamine (LacDiNAc) based on galactose oxidase treatment. Beilstein J Org Chem. 2012;8:712–25.

33. Lutolf MP, Hubbell J a. Synthesis and physicochemical characterization of end-linked poly(ethylene glycol)-co-peptide hydrogels formed by Michael-type addition. Biomacromolecules. 2003;4:713–22.

34. Margareth RC, Raimar L. Simulated biologic fluids with possible application in dissolution testing. Dissolutio Technol. 2011;15–28.

35. Kaufman GN. Therapeutic potential of endothelin receptor type A and bradykinin receptor B1 dual antagonism in osteoarthritis treatment. Univ. Montr. 2010.

36. Ekundi-Valentim E, Santos KT, Camargo E a, Denadai-Souza a, Teixeira S a, Zanoni CI, et al. Differing effects of exogenous and endogenous hydrogen sulphide in carrageenan-induced knee joint synovitis in the rat. Br J Pharmacol. 2010;159:1463–74.

37. Morgen M, Tung D, Boras B, Miller W, Malfait AM, Tortorella M. Nanoparticles for improved local retention after intra-articular injection into the knee joint. Pharm Res. 2013;30:257–68.

38. Alonso MJ, Garcia-Fuentes M. Nano-Oncologicals: New Targeting and Delivery Approaches. 2014.

39. Clemons TD, Viola HM, House MJ, Hool LC, Iyer KS. The Design and Testing of Multifunctional Nanoparticles for Drug Delivery Applications. 2016.

40. Rothenfluh DA, Bermudez H, Neil CPO, Hubbell JA. Biofunctional polymer nanoparticles for intra-articular targeting and retention in cartilage. 2008;7:1–7.

41. Prince A. Development of in situ Forming Hydrogels for Intra-articular Drug Delivery. 2019.

42. Fezai M, Senovilla L, Jemaà M, Ben-Attia M, Ben-Attia M. Analgesic, Anti-Inflammatory and Anticancer Activities of Extra Virgin Olive Oil. J Lipids. 2013;2013:1–7.

43. Moghimipour E, Salimi A, Karami M, Isazadeh S. Preparation and characterization of dexamethasone microemulsion based on pseudoternary phase diagram. Jundishapur J Nat Pharm Prod. 2013;8:105–12.

44. Chime S a, Kenechukwu FC, Attama a a. Nanoemulsions — Advances in Formulation, Characterization and Applications in Drug Delivery. 2014;

45. Mourdikoudis S, Liz-Marzán LM. Oleyamine in Nanoparticle Synthesis. Chem Mater. 2013;25:1465.

46. Ghosh P, Guidolin D. Potential mechanism of action of intra-articular hyaluronan therapy in osteoarthritis: Are the effects molecular weight dependent? Semin Arthritis Rheum. 2002;32:10–37.

47. El-Hakim IES, Abdel-Hamid IS, Bader a. Tempromandibular joint (TMJ) response to intra-articular dexamethasone injection following mechanical arthropathy: A histological study in rats. Int J Oral Maxillofac Surg. 2005;34:305–10.

48. Chen WS, Cao Z, Leffler H, Nilsson UJ, Panjwani N. Galectin-3 inhibition by a small-molecule inhibitor reduces both pathological corneal neovascularization and fibrosis. Investig Ophthalmol Vis Sci. 2017;58:9–20.

49. Chernyshev VS, Rachamadugu R, Tseng YH, Belnap DM, Jia Y, Branch KJ, et al. Size and shape characterization of hydrated and desiccated exosomes. Anal Bioanal Chem. 2015;407:3285–301.

50. Brown AC, Barker TH. Fibrin-based biomaterials: Modulation of macroscopic properties through rational design at the molecular level. Acta Biomater. 2014;10:1502–14.

51. Snyder TN, Madhavan K, Intrator M, Dregalla RC, Park D. A fibrin/hyaluronic acid hydrogel for the delivery of mesenchymal stem cells and potential for articular cartilage repair. J Biol Eng. 2014;8:10.

52. Vilela C, Correia C, Oliveira JM, Sousa RA, Espregueira-Mendes J, Reis RL. Cartilage repair using hydrogels: a critical review of in vivo experimental designs. ACS Biomater Sci Eng. 2015;150813111234008.

53. Avner Yayon, Meital Ben-Dayan Bloch, Ezequiel Wexselblatt, Ron Arbel GA. A Chondrogenic Fibrin-HA Hybrid Proteoglycan for OA Pain Relief and Cartilage Preservation from Bench to Clinics. 2017.

54. Chemistry and Biology of Hyaluronan. H.G. Garg and C.A. Hales (Ed.) 2004. p. 624, Amsterdam: Elsevier Science.

55. Masuko K, Murata M, Yudoh K, Kato T, Nakamura H. Anti-inflammatory effects of hyaluronan in arthritis therapy: Not just for viscosity. Int J Gen Med. 2009;2:77–81.

56. Fraser JR, Laurent TC, Laurent UB. Hyaluronan: its nature, distribution, functions and turnover. J Intern Med. 1997;242:27–33.

57. Moreland LW. Intra-articular hyaluronan (hyaluronic acid) and hylans for the treatment of osteoarthritis: mechanisms of action. Arthritis Res Ther. 2003;5:54–67.

58. Lugovskoy E.V. Molecular Mechanisms of formation and degradation of fibrin. Komissarenko S.V. (Ed.) 2003. p. 223. Kyiv: Naukova Dumka.

59. Chernysh IN, Nagaswami C, Weisel JW. Visualization and identification of the structures formed during early stages of fibrin polymerization Visualization and identification of the structures formed during early stages of fibrin polymerization. 2011;117:4609–14.

60. Weigel PH, Frost SJ, LeBoeuf RD, McGary CT. The specific interaction between fibrin(ogen) and hyaluronan: possible consequences in haemostasis, inflammation and wound healing. 1989;143:248–61; discussion 261-4, 281–5.

61. LeBoeuf RD, Raja RH, Fuller GM, Weigel PH. Human fibrinogen specifically binds hyaluronic acid. J Biol Chem. 1986;261:12586–92.

62. Gobbo S, Petrella RJ. WO 2007/131546. Hyaluronic acid binary mixtures and therapeutic thereof. 2007.

63. Mehta DP, Shodhan K, Modi RI, Ghosh PK. Sodium hyaluronate of defined molecular size for treating osteoarthritis. Curr Sci. 2007;92:209–13.

64. Castor BCW. Hyaluronic Acid in Human Synovial Effusions; A Sensitive Indicator of Altered Connective Tissue Cell Function During Inflammation. Arthritis Rheum. 1966;9:783–94.

65. Francis W and Marder J. Increased resistance to plasmic degradation of fibrin with highly crosslinked alpha-polymer chains formed at high factor XIII concentrations. Blood. 1988;71.

66. Muszbek L, Bereczky Z, Bagoly Z, Komáromi I, Katona É. Factor XIII: a coagulation factor with multiple plasmatic and cellular functions. Physiol Rev. 2011;91:931–72.

67. Tsurupa G, Yakovlev S, McKee P, Medved L. Noncovalent interaction of alpha(2)-antiplasmin with fibrin(ogen): localization of alpha(2)-antiplasmin-binding sites. Biochemistry. 2010;49:7643–51.

68. Palmer M, Stanford E, Murray MM. The effect of synovial fluid enzymes on the biodegradability of collagen and fibrin clots. Materials. 2011;4:1469–82.

69. Aya KL, Stern R. Hyaluronan in wound healing: Rediscovering a major player. Wound Repair Regen. 2014;22:579–93.

70. Finelli I, Chiessi E, Galesso D, Renier D, Paradossi G. A new viscosupplement based on partially hydrophobic hyaluronic acid: A comparative study. Biorheology. 2011;48:263–75.

71. Choi B, Loh XJ, Tan A, Loh CK, Ye E. Introduction to In Situ Forming Hydrogels for Biomedical Applications. 2015.

72. Park SH, Cui JH, Park SR, Min BH. Potential of fortified fibrin/hyaluronic acid composite gel as a cell delivery vehicle for chondrocytes. Artif Organs. 2009;33:439–47.

73. Zhang Y, Heher P, Hilborn J, Redl H, Ossipov D. Hyaluronic acid-fibrin interpenetrating double network hydrogel prepared in situ by orthogonal disulfide cross-linking reaction for biomedical applications. Acta Biomater. 2016;38:23–32.

74. Janmey P a, Winer JP, Weisel JW. Fibrin gels and their clinical and bioengineering applications. J R Soc Interface. 2009;6:1–10.

75. Frost SJ, Weigel PH. Binding of hyaluronic acid to mammalian fibrinogens. BBA - Gen Subj. 1990;1034:39–45.

76. Matsuzaki T, Matsushita T, Tabata Y, Saito T, Matsumoto T, Nagai K, et al. Intra-articular administration of gelatin hydrogels incorporating rapamycin-micelles reduces the development of experimental osteoarthritis in a murine model. Biomaterials. 2014;35:9904–11.

77. Türker S, Erdoğan S, Özer AY, Ergün EL, Tuncel M, Bilgili H, et al. Scintigraphic imaging of radiolabelled drug delivery systems in rabbits with arthritis. Int J Pharm. 2005;296:34–43.

78. Webber MJ, Matson JB, Tamboli VK, Stupp SI. Controlled release of dexamethasone from peptide nanofiber gels to modulate inflammatory response. Biomaterials. 2012;33:6823–32.

79. Mosesson MW, Siebenlist KR, Hernandez I, Lee KN, Christiansen VJ, Mckee P a. Evidence that a2-antiplasmin becomes covalently ligated to plasma fibrinogen in the circulation: A new role for plasma factor XIII in fibrinolysis regulation. J Thromb Haemost. 2008;6:1565–70.

80. Chen HY, Liu F-T, Yang R-Y. Roles of galectin-3 in immune responses. Arch Immunol Ther Exp. 2005;53:497–504.

81. Page-McCaw A, Ewald AJ, Werb Z. Matrix metalloproteinases and the regulation of tissue. Nat Rev Mol Cell Biol. 2007;8:221–33.

82. ClinicalTrials NCT02407041. An Open-Label, Phase 2a Study to Evaluate Safety and Efficacy of GR-MD-02 for Treatment of Psoriasis. 2018.

83. Clinical Trials NCT02257177. RCT (Randomized Control Trial) of TD139 vs Placebo in HV's (Human Volunteers) and IPF Patients Purpose. 2017.

84. Santos JM, Bárcia RN, Simões SI, Gaspar MM, Calado S, Agua-Doce A, et al. The role of human umbilical cord tissue-derived mesenchymal stromal cells (UCX®) in the treatment of inflammatory arthritis. J Transl Med. 2013;11:18.

85. Hsieh TJ, Lin HY, Tu Z, Huang BS, Wu SC, Lin CH. Structural basis underlying the binding preference of human galectins-1, -3 and -7 for Galβ1-3/4GlcNAc. PLoS One. 2015;10:1–19.

86. Hsieh T, Lin H-Y, Tu Z, Lin T-C, Wu S, Tseng Y, et al. Dual thio-digalactoside-binding modes of human galectins as the structural basis for the design of potent and selective inhibitors. Sci Rep. 2016;6:29457.

87. Giuseppe Cirino CC. Thrombin Functions as an Inflammatory Mediator through Activation o f Its Receptor. J Exp Med. 1996;183.

88. Optical Measurement of Surface Topography. Leach R (Ed.). 2012. p. 323. Springer-Verlag: Berlin Heidelberg.

Supporting Information

Nataliya Storozhylova[1,3], José Crecente-Campo[1], David Cabaleiro[2], Luis Lugo[2], Christophe Dussouy[3], Sandra Simões[4], Madalena Monteiro[5], Cyrille Grandjean[3], María J. Alonso[1]

Rheological data and 3D roughness parameters of *in situ* non-fortified and fortified HA-fibrin hydrogels with loaded NCs

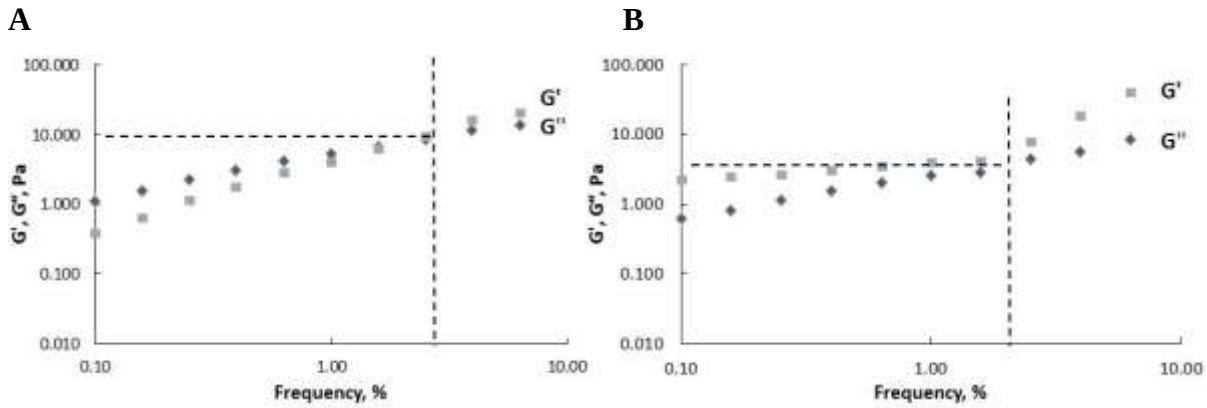

Figure S1. Deformation point detection by the response of elastic (G') and viscous (G") moduli in HA-fibrin **(A)** and fortified HA-fibrin systems **(B)** with 30% loaded NCs as a function of frequency at torque 0.5 μN·m. Fibrinogen was always taken at 1.5 mg/mL concentration, activity of thrombin = 2 NIH-U/mL. The measurements were carried out at 37 °C. Expressed as mean ± SD; n = 3.

Hydrogels 3D roughness parameters (S_{sk}, which represents the degree of symmetry of the surface heights distribution about the mean plane, and S_{ku}, which indicates the nature of the height distribution) [88] are shown in **Table S1**.

Table S1. Experimental roughness results from different zoomed areas of hydrogel samples. $S_{sk} = 0$: Symmetrical about the average line (normal distribution), $S_{sk} > 0$: skewed downward relative to the average line $S_{sk} < 0$: skewed upward relative to the average line. $S_{ku} = 3$: normal distribution, $S_{ku} > 3$: the height distribution is spiked. $S_{ku} < 3$: the form of the surface roughness height distribution is squashed.

Sample	3D Roughness Parameters	
	S_{sk}	S_{ku}
HA-fibrin hydrogel		
Area 1 (Field of View 97×108 μm^2)	0.01	3.00
Area 2 (Field of View 63×73 μm^2)	0.19	3.42
Area 3 (Field of View 53×61 μm^2)	-0.09	3.00
HA-fibrin hydrogel + 30% NCs		
Area 1 (Field of View 98×124 μm^2)	-0.17	3.08
Area 2 (Field of View 103×129 μm^2)	-0.30	3.17
Area 3 (Field of View 87×109 μm^2)	-0.61	3.23
Fortified HA-fibrin hydrogel		
Area 1 (Field of View 126×132 μm^2)	0.25	3.11
Area 2 (Field of View 103×103 μm^2)	0.62	7.21
Area 3 (Field of View 74×94 μm^2)	0.36	3.51
Fortified HA-fibrin hydrogel + 30% NCs		
Area 1 (Field of View 97×136 μm^2)	0.34	7.28
Area 2 (Field of View 101×131μm^2)	-0.03	2.67
Area 3 (Field of View 91×110 μm^2)	0.39	4.47

Table S2. Mean pore size and depth of the different hydrogel compositions.

Sample	Mean pore diameter (μm)	Depth (μm)
HA-fibrin hydrogel	4.23 ± 0.89	1.07 ± 0.18
HA-fibrin hydrogel + 30% NCs	7.29 ± 1.23	0.70 ± 0.17
Fortified HA-fibrin hydrogel	3.26 ± 1.01	1.07 ± 0.41
Fortified HA-fibrin hydrogel + 30% NCs	4.88 ± 1.12	0.98 ± 0.12

***In vitro* drug release from NCs loaded hydrogels**

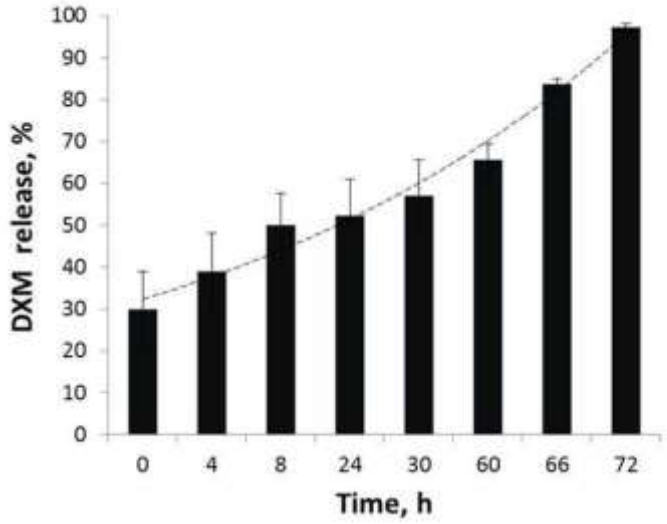

Figure S2. *In vitro* release of the model drug (DXM) from HA-fibrin hydrogel with 30% loaded NCs to simulated synovial fluid, incubated at 37 °C during 72 h. Expressed as mean ± SD; n = 3.

Histopathological data

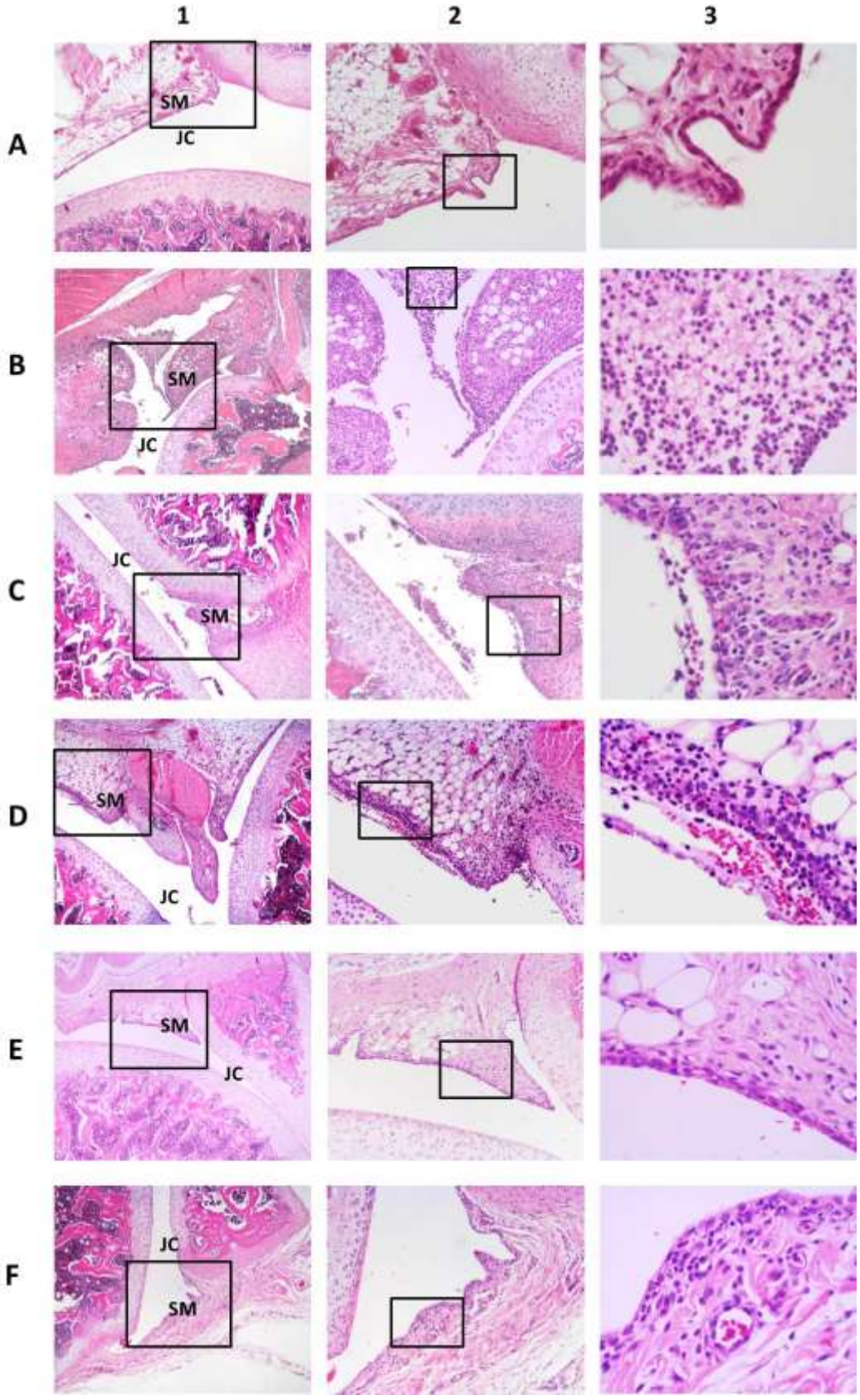

Figure S3. Microphotographs of the knee joints of rats, injected with tested materials, stained with haematoxylin and eosin; low (40×), medium (100×) and high (400×) magnification

(columns 1, 2 and 3 respectively). The square areas in the images reveal the amplified regions of the photograph. Groups: saline control (row **A**), carrageenan control (row **B**), blank NCs + carrageenan (row **C**), Gal-3i NCs + carrageenan (row **D**), blank NCs + gel (row **E**) and Gal-3i NCs + gel + carrageenan (row **E**). **SM**: synovial membranes; **JC**: joint cavity.